FAST MARCHING METHOD TO CORRECT FOR REFRACTION IN ULTRASOUND COMPUTED TOMOGRAPHY

Shengying Li[†], Klaus Mueller[†], Marcel Jackowski[‡], Donald P. Dione*, Lawrence H. Staib[‡]

[†] Department of Computer Science, Stony Brook University
[‡] Department of Diagnostic Radiology, Yale University
* Ultrasound Detection Systems

ABSTRACT

A significant obstacle in the advancement of Ultrasound Computed Tomography has been the lack of efficient and precise methods for the tracing of the bent rays that result from the interaction of sound with refractive media. In this paper, we propose the use of the Fast Marching Method (FMM) to solve the eikonal equation which governs the propagation of sound waves. The FMM enables us to determine with great accuracy and ease the distorted paths that the sound rays take from an emitter to the receivers. We show that knowledge of the accurate path proves crucial for an object reconstruction at high fidelity and accurate geometry. We employ a two-phase approach with an iterative method, SART, to faithfully reconstruct two tissue properties relevant in clinical diagnosis, such as mammography: speed of sound and sound attenuation. We demonstrate our results by ways of a newly designed analytical ultrasound breast phantom.

1. INTRODUCTION

Ultrasound computed tomography (UCT) has a long history and particular promise in the imaging of the breast. However, the reconstruction of these images poses significant challenges. UCT is susceptible to refraction effects, making it difficult to reconstruct images faithfully. The acoustic ray direction is bent when ultrasound passes from one medium to another medium with a change in the acoustic index of refraction, according to Snell's law for refraction. For example, the large subcutaneous fat layer in the breast [17][18] causes a refractive effect that can significantly distort the ultrasound ray direction and eventually cause spatial distortion and intensity artifacts in the resulting images. Diffraction is another complication typically addressed by diffraction tomography methods [7] but it is based on the weak scattering assumption [12], which is violated by the strongly refracting fat layers in the breast. In this work, we focus on correcting the artifacts stemming from refraction. Previous work has either not modeled bent rays at all or has inadequately eliminated bent ray distortion effects and failed to faithfully reproduce tissue properties in UCT. Furthermore, prior methods have been computationally expensive, limiting their extendibility to three dimensions.

To advance the state of the art in these respects, we introduce the concept of wave-based ray propagation models into UCT imaging, accurately taking into account the refractive phenomena. For this, we model the eikonal equation, which governs the movement of a wave front from emitters to receivers, using the Fast Marching Method (FMM), described by Sethian [15]. With this method, the wave arrival time for each grid point can be extracted, and the accurate ray direction for an arbitrary point can be derived by searching for the minimum path in the Time-Of-Flight field between the point and the emitter. The FMM has become quite popular in recent years in computer graphics and computer vision, enabling accurate distance transforms, segmentation shape recognition, and others. In this paper, we demonstrate that the FMM also represents a promising method for the efficient and accurate modeling of the propagation of acoustic waves in a refractive media.

Our paper is structured as follows. In section 2, we first review some related work. Section 3 then provides the theoretical background on the models we propose and section 4 describes the implementation details of our algorithm for the modeling of non-linear rays for the reconstruction. Section 5 then presents and discusses our experimental results. Finally, we conclude and describe future directions of research in section 6.

2. RELATED WORK

Starting from the late 70's and early 80's, experimental work in UCT has been driven by the need for real-time data acquisition and display. While recent work by Duric [8] shows promise and discusses the effect, that a scatter field with reflection and refraction properties has, the reconstruction algorithms discussed there are still limited to the straight-ray assumption.

To solve the problems associated with bent rays, Meyer [10] proposed a method to correct for the multi-path errors using a parametric multi-path modeling and estimation scheme, while Pan and Liu [14] proposed methods to correct for refractive errors by scanning a small area around the straight line-of-sight and then using the maximum, sum or average of the area to measure the attenuation. Several researchers [2][11] explored the use of ray-tracing, via ray-linking, in an iterative reconstruction framework to improve the UCT image quality. Andersen [2] proposed a ray rebinning method to generate new projection data, while Denis [5] compared several methods for ray-tracing, showing that substantial improvement over straight ray methods can be achieved for moderately refracting fields. There still remains a need for further improvement, especially in terms of computational speed and accuracy.

3. THEORETICAL BACKGROUND

3.1. Reconstruction Algorithm

Classical tomography reconstruction algorithms using Filtered Backprojection are based on the Radon theorem and can not take into account bent rays. Therefore, similar to other UCT researchers, we employ an algebraic reconstruction approach, SART [1]. Given the projection data p_i, SART updates a pixel v_j in iteration k according to the following equation:

$$v_j^k = v_j^{k-1} + \lambda \sum_{p_i \in P\varphi} c_i w_{ij} / \sum_{p_i \in P\varphi} w_{ij}; \quad c_i = (p_i - \sum_{i=1}^{N} w_{il} v_l^{k-1}) / \sum_{l=1}^{N} w_{il}$$

Here the w-terms relate the pixels to the data and are determined by the interpolation function. The correction/update factor c_i is computed by subtracting the result of a discrete ray integration (within the grid constructed at iteration $(k$-1$)$) from the physical integration acquired at receiver i. In our case, due to the refraction effects, the rays are non-linear. SART is a block-based algorithm, i.e., a grid update occurs after all rays for a given source (emitter) have been traced and the correction factors computed.

3.2. Solving the Eikonal Equation with the FMM

As discussed above, our approach advocates an alternative way to solve the bent-ray problem by directly simulating the acoustic sound wave propagation. Bent rays can be computed by solving the eikonal equation [13]:

$$(\partial t / \partial x)^2 + (\partial t / \partial y)^2 + (\partial t / \partial z)^2 = 1 / F^2(x, y, z) \qquad (1)$$

on a discretized grid of points. Traditionally, equations such as equation 1 are solved by iterative methods, which can be computationally expensive. To solve the eikonal equation more efficiently, we employ the Fast Marching Method (FMM), originally proposed by Tsitsiklis [19]. The FMM is related to Dijkstra's method [6], which is a classical algorithm for identifying the shortest path in a network of links. The FMM is a single-pass, upwind finite difference scheme, which produces the correct viscosity solution to the eikonal equation. It depends on a causality condition based on the ordering of the upwinding [15].

In equation 1, F is called the speed term and is a measure of the local sound conductance properties. The FMM computes for every voxel (x,y,z) the time $T(x,y,z)$ at which the wave has traversed it. As the wave front proceeds across the grid, the FMM selects the voxel (x,y,z) in the narrow band of voxels (situated immediately upwind from the current wave boundary) which minimizes the time increment, given the values of its neighbors and their speed values. The result of the FMM is the Time Of Flight (TOF) image. There is one such image for each emitter.

The original FMM solves the eikonal equation by using only first-order finite difference. This will lead to inaccuracies at high curvature boundaries. For a more accurate approximation of equation 1, we use the High Accuracy Fast Marching Method (HAFMM) [4]. It employs a second-order approximation to the partial derivative in (1), such as

$$\partial t / \partial x = (3t(x, y, z) - 4t(x - 1, y, z) + t(x - 2, y, z)) / 2,$$

but it also requires accurate second-order estimates for initialization around the propagation seed points (emitter locations).

Once the propagation is complete, we use the resulting TOF image to calculate the path of the rays from the receivers back to the emitter. The TOF image allows us to locally compute the ray direction vectors, given by the TOF image gradients, ensuring that a given ray will not miss the emitter. Our method thus eliminates the need for the ray linking and path assembly of earlier approaches. Figure 1 shows the acoustic ray paths from 31 receivers, which are distorted when passing through the object. White curves represent the wave front at different times. The yellow lines are the straight rays between emitter and receiver and the red lines represent the curved-rays obtained via HAFMM.
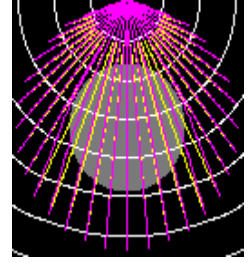
Figure 1. Curved-ray (red) and straight ray (yellow) with the FMM.

3.3. Ultrasound Breast Modeling

In the area of computational tomography, there are a number of existing breast phantoms [3][16]. However, they are usually too complex, and some of the structures are not perceptibly differentiated in an UCT image. Therefore, a simple, numeric UCT breast phantom is proposed, as shown in Figure 2.

(a) anatomy (from info.med.yale.edu)

(b) phantom (left: vertical slice; right: horizontal slice.)
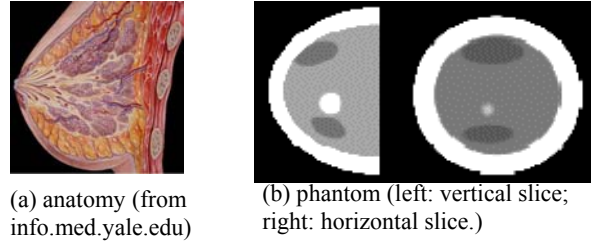
Figure 2. Breast anatomy and phantoms.

Our UCT breast phantom is modeled using a half ellipse, and is composed of two main layers: an outer thick layer of fat and an inner layer of tissue. In the inner layer of the tissue, several lesions are shown as small ellipses, and smaller abnormalities modeled as tiny spheres are inserted. Keeping the shape unchanged and adjusting the values of the phantoms, we can simulate a sound velocity (sound conductance) phantom and an attenuation phantom separately. See Table 1 for the clinical values used in the phantoms. Both the sound velocity and the attenuation properties of tissue provide valuable diagnostic information. The analytical geometric description of the elliptical primitives allows for easy analytical modeling of refracted ray paths and their path integration in the simulation of projection data. We have not used real data at this time, in order to isolate the aliasing and distortion effects purely due to the non-linear, refracted rays (as opposed to higher-order scattering noise).

Ultrasound Properties	Tissue	Fat	Large Lesions	Small Lesions
Velocity	1475 m/s	1375 m/s	1560 m/s	1530 m/s
Attenuation	50	15	60 or 30	70

Table 1. Our phantom's breast ultrasound properties

4. METHODOLOGY

Our novel contribution is to combine SART with FMM to find the accurate ray directions by wave propagation. In this way, we can avoid the complicated bent-ray computations that previous UCT

reconstruction algorithms had to deal with, replacing them with the simple and linear computations embodied by the FMM.

In this research, we implemented both FMM and HAFMM. We use a binary heap to quickly find the voxel with the smallest postulated wave arrival time in the narrow band of the advancing wave front. This voxel's wave arrival value is then written to the Time-Of-Flight (TOF) image, its neighbors and their arrival times are updated in the heap. Note that a translation table with double pointers, as is further described in [15][4] is used in order to quickly map the spatial domain voxels to the heap voxels.

Our framework itself can be decomposed into a two-phase algorithm. In phase 1, we iteratively reconstruct the sound velocity (SV) image from the TOF data collected at the receivers, and in phase 2, we use this SV image to guide the non-linear rays for the iterative reconstruction of the sound attenuation (SA) image from the attenuation data collected at the receivers. Both phases use SART as the iterative reconstruction engine. Note that the SA image is easy to reconstruct once an accurate SV image is available to guide the distorted rays, provided the gradients are faithfully reconstructed using good interpolation filters. Our algorithm proceeds as follows:

Initialize image
Until convergence, loop
 Randomly select an emitter E
 Propagate waves using sound velocity image SV
 - Record TOF at each pixel, including receivers
 - Trace back from receivers to E with TOF gradient
 - Compute the ray length L
 Compute correction factors

 - $\Delta TOF = (TOF_{simulated} - TOF_{collected})/L$

 Back project ΔTOF along ray direction
 Update SV image according to ΔTOF at each pixel.

Figure 3. the pipeline of the FMM-based-SART.

For the SV update step, we use the relationship $v = d/t$. Here, d is the diameter of a spherical pixel (we assume spherical pixel to achieve direction independence and use d = 1). The following equation is employed:

$$SV^{k+1} = d/(d/SV^k + \sum_{rays} \Delta TOF)$$

One iteration completes after all emitters have been processed once, and the iterations continue until the difference between the TOF image at the receiver positions and the collected TOF data there becomes smaller than a threshold. Usually, this requires 3 to 4 iterations. The reconstruction of SA image is similar, only now the SV image remains constant and with it the ray paths and their lengths. Note, the algorithm requires the estimation of good gradients. For this, we employ B-splines, which have previously shown to work well in refractive media [5][9].

The velocity of a grid point, stored in the SV image and used in the wave propagation step of the reconstruction, depends heavily on the reconstructed value at that point obtained from previous iterations. To obtain the accurate speed value, we investigated two different approaches: *fixed speed update* and *data-driven speed update*.

Fixed speed update means that the speed update is applied directly to the pixel, without further scaling. $\quad F = k \cdot SV (2)$

Data-driven speed update means that the speed update is normalized in the following equation:

$$F = k\left(F_{min} + \frac{SV - SV_{cur-min}}{SV_{cur-max} - SV_{cur-min}}\left(F_{max} - F_{min}\right)\right) (3)$$

In equations 2 and 3, k is a constant scale factor, $SV_{cur-min}$ and $SV_{cur-max}$ are the speed extrema of current iteration, F_{min} and F_{max} are the inherent speed extrema of the object, and F is the resulting propagation speed.

The fixed speed update strategy is intuitive, considering the fact that the values in the SV image represent material properties, and acoustic rays always have the same speed in a specific material. However, it can suffer from the problem that the shape of the organ is distorted by the first few iterations' speed value, when the correct value has not been constructed yet.

Data-driven speed update is introduced to solve this problem in the iterative reconstruction algorithm. In this method, we assume that in the initial iterations the pixel's absolute value may not be accurate but the overall geometric information has been quickly formed and recorded in the grid point's relative values. The normalization ensures a fast ascent of the solution at early iterations when SV values are small.

For the construction of the SA image, the TOF image can either be computed beforehand, or on the fly when storage is excessive, using the FMM on the reconstructed SV image. The input data are now the collected attenuation data, one set for each emitter, and SART proceeds as usual for each randomly chosen emitter position, using the rays guided by the corresponding TOF image, but now updating the attenuation volume.

5. EXPERIMENTS AND RESULTS
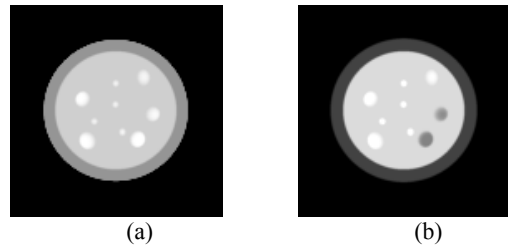
(a)   (b)
Figure 4. Breast phantom
(a) ultrasound velocity; (b) ultrasound attenuation.

Our experiments are based on a simulated computer phantom with a matrix size of 128x128, and the quantitative parameters are given in Table 1. The phantoms are shown in Figure 4, holding lesions with diameters from 2 to 8 pixels. The ultrasound TOF and attenuation phantoms share the same geometry. Our simulation assumes a spherically radiating sound emission, using 256 emitter/receiver positions in a circle. The resolution of the reconstructed image matches the size of the phantom images. More emitter/receiver pairs enable higher resolution. Reconstruction costs about 60 seconds for 3 iterations using a 2.8GHz Pentium 4.
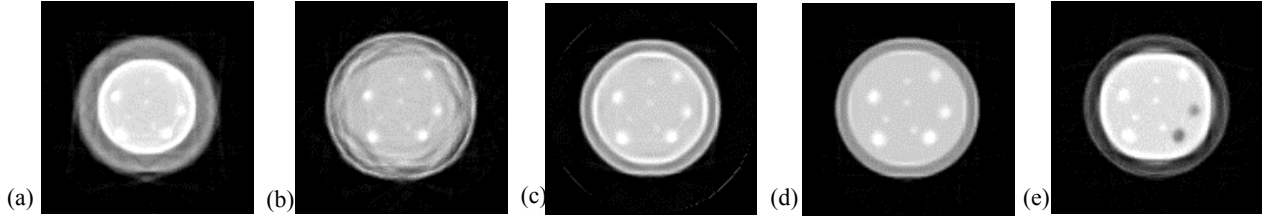
Figure 5: Reconstructed images: (a) straight ray SV image, HAFMM; (b) nonlinear ray SV with fixed speed, HAFMM; (c) nonlinear ray SV with relaxed speed, FMM; (d) nonlinear ray SV with relaxed speed, HAFMM; (e) attenuation image.

For the velocity phantom, the reconstruction results are given in Figure 5 (a)-(d). With HAFMM, the reconstructed image obtained with linear rays is shown in (a) and non-linear rays in (b) and (d). For the non-linear ray reconstruction, we further compare the results obtained for the different speed strategies: fixed speed in (b) and data-driven speed in (d). We calculate the error as the average absolute intensity difference for all grid points between the reconstructed image and the original phantoms. The use of only straight rays distorts the image with an error of 25%. Because refraction is ignored, the size of the phantom's regions grows or shrinks dramatically. When correcting for refraction, the speed strategy has a large impact on the resulting image accuracy. The data-driven relaxed speed results in a better estimation of the original image (error of 3%), while the fixed speed strategy over-corrects for refraction with an error of 19%.

The image achieved using FMM is shown in Figure 5(c), with the error of 10%. HAFMM in (d) is more accurate than FMM in (c), since the HAFMM includes second-order curvature information when solving the eikonal equation. This means that boundaries where refraction occurs are better determined.

Finally, the attenuation phantom reconstruction results are presented in Figure 5(e). It is based on the nonlinear ray paths determined in the SV phantom reconstruction shown in 5(d), using the HAFMM. The attenuation image recovers both intensity and shape accurately with an error of less than 7%.

6. CONCLUSIONS AND FUTURE WORK

In this paper, a new method for UCT image reconstruction taking into account refraction was proposed. The key observation behind this method is that the up-winding Fast Marching Method (FMM) can determine the first-arriving phase in a continuous medium. It also provides computational efficiency in determining the accurate paths of the non-linear rays. We proposed two speed mechanisms for the FMM to trace the refractive rays: fixed speed and data-driven relaxed speed. Our method is applicable in any UCT imaging situation in a moderate refractive media. UCT simulations, using a synthetic breast phantom, have demonstrated that the continuous wave propagation in HAFMM with data-driven relaxed speed achieves an accurate determination of the non-linear ray paths and provides much better fidelity in the image reconstruction. The reconstructed image quality improves by an order of magnitude compared to the pure straight ray method.

In the future, we plan to exploit these novel technologies using real UCT data and extend them to a 3-dimensional refraction reconstruction.

ACKNOWLEDGMENTS

REFERENCES

[1] A. H. Andersen and A. C. Kak, "Simultaneous algebraic reconstruction technique (SART)," *Ultrason. Img.,* 6: p. 81–94, 1984.

[2] A. H. Anderson, "A Ray Tracing Approach to Restoration and Resolution Enhancement in Experimental Ultrasound Tomography", *Ultrason. Img.,* 12: p. 268-291, 1990.

[3] K. Bliznakova, Z. Bliznakov, V. Bravou, et.al., "A Three-Dimensional Breast Software Phantom for Mammography Simulation", *Phys. Med. Biol.* 48 3699-3719, 2003.

[4] J. A. Barentzen, "On the Implementation of Fast Marching Methods for 3D Lattices", *Tech. report*, Tech. Univ. of Denmark, 2001.

[5] F. Denis, O. Basset, G. Gimenez, "Ultrasonic Transmission Tomography in Refracting Media: Reduction of Refraction Artifacts by Curved-Ray Techniques", *IEEE Trans. Med. Img.* 14: p.173-88, 1995.

[6] E. W. Dijkstra, "A note on two problems in connection with graphs", *Numeric Mathematics*, 1: p.269 – 271, 1959.

[7] K. T. Ladas, A. J. Devaney, "Application of an ART in an Experimental Study of Ultrasonic Diffraction Tomography", *Ultrason. Img.*, 15: p. 48-58, 1993.

[8] N. Duric, P. Littrup, A. Babkin, et.al., "Development of Ultrasound Tomography for Breast Imaging: Technical Assessment", *Am. Assoc. Phys. Med.*, 32(5): p1375-1386, 2005.

[9] S. Li, K. Mueller, "Spline-Based Gradient Filters for High-Quality refraction Computations in Discrete Datasets", *Symp. of EuroVis*, Leads, 2005.

[10] C. R. Meyer, T. L. Chenevert, P. L. Carson, "A Method for Reducing Multipath Artifacts in Ultrasonic Computed Tomography", *J. Acoust. Soc. Am.*, 72(3): p. 820-823, 1982.

[11] S. J. Norton, "Computing ray Trajectories between Two Points: A Solution to the Ray-linking Problem", *Optical Soc. of America*, 4(10): p. 1919-1922, 1987.

[12] X. Pan., "Unified Reconstruction theory for Diffraction Tomography, with Consideration of Noise Control", *J. Opt. Soc. Am*. A, 15: p. 2312-2326, 1998.

[13] V. Pereyra, "Ray Tracing Methods for Inverse Problems", *Inverse Problems,* 16: R1-R35, 2000.

[14] K. M. Pan, C. N. Liu, "Tomographic Reconstruction of Ultrasonic Attenuation with Correction for Refractive Errors", *IBM J. Res. Develop.*, 25(1): p. 71-82, 1981.

[15] J. A. Sethian, "Level Set Methods and Fast Marching Methods: Evolving Interfaces in Geometry, Fluid Mechanics, Computer Vision, and Material Science", 2nd Edit., *Cambridge Monographs on Applied and Computational Mathematics*, 1999.

[16] P. Taylor, R Owens and D. Ingram, "Simulated Mammography Using Synthetic 3D Breasts digital Mammography", *Proc. 4th Int. Workshop on Digital Mammography*, Nijnegen, p. 283-90, 1998.

[17] [G. E. Trahey, P. D. Freiburger, L. F. Nock, D. C. Sullivan, "In Vivo Measurement of Ultrasonic Beam Distortion in the Breast", *Ultrason. Img.*, 13: p. 71-90, 1999.

[18] Q. Zhu, B. D. Steinberg, "Wavefront Amplitude Distribution in the Female Breast", *J. Acous. Soc. of America*, 96(1): p. 1-9, 1996.

[19] J. Tsitsiklis, "Efficient algorithms for globally optimal trajectories". *IEEE Trans. on Automatic Control*, 40(9):1528–1538, 1995.